Aeroelasticity of compliant span morphing wings

IOP Publishing Smart Materials and Structures
Smart Mater. Struct. **27** (2018) 105052 (16pp) https://doi.org/10.1088/1361-665X/aad219

Aeroelasticity of compliant span morphing wings

Rafic M Ajaj[1] **and Michael I Friswell**[2]

[1] College of Engineering, United Arab Emirates University, Al Ain, United Arab Emirates
[2] College of Engineering, Swansea University, Swansea SA1 8EN, United Kingdom

E-mail: raficajaj@uaeu.ac.ae

Received 11 April 2018, revised 3 July 2018
Accepted for publication 9 July 2018
Published 21 September 2018

Abstract

A low-fidelity aeroelastic model is developed to study the dynamic behaviour of uniform, cantilever span morphing wings. The wing structure is modelled using the shape functions of the bending and torsional modes of a uniform cantilever wing according to the Rayleigh–Ritz method. Theodorsen's unsteady aerodynamic theory is used to model the aerodynamic loads. A Padé approximation for the Theodorsen's transfer function is utilised to allow time-domain simulation and analysis. The sensitivity of the aeroelastic behaviour of span morphing wings to different geometric parameters and mechanical properties is considered. Furthermore, the impact of morphing rate on the aeroelastic behaviour is studied. Finally, the use of two novel span morphing concepts for flutter suppression is assessed.

Keywords: span morphing, compliant wing, flutter suppression, actuation, aeroelasticity

(Some figures may appear in colour only in the online journal)

Nomenclature

$\hat{a}$	normalised pitch axis location with respect to half chord ($\hat{a}=-1$ leading edge, $\hat{a}=1$ trailing edge)
b	wingspan
c	chord of the aerofoil/wing
$\overline{EI}$	bending rigidity
$\overline{GJ}$	torsional rigidity
$h(y)$	bending shape function
I'_{ea}	mass moment of inertia around the elastic axis
l	wing semi-span
L'	lift per unit span
L	equivalent lift force
LE	leading edge
m'	mass per unit span
M'_{ea}	pitching moment per unit span around the elastic axis
M_{ea}	equivalent pitching moment around the elastic axis
r_θ	radius of gyration
s	Laplace variable
t	time
T	total kinetic energy
U	total potential energy
V	true airspeed
x_θ	distance between elastic axis and centre of gravity
w	plunge displacement at elastic axis
y	spanwise location measured relative to the wing root
θ	pitch angle
$\phi(y)$	torsion shape function
ρ	air density

Subscripts

t	wingtip

Superscripts

. first time derivative

.. second time derivative

1. Introduction

Aircraft with large wingspans have higher aerodynamic efficiency but reduced manoeuvrability margin when compared to those with low aspect ratio [1]. A span morphing wing can combine the advantages of both design (high aspect ratio and low aspect ratio) allowing one aircraft to effectively perform different types of missions [2–4]. Ajaj *et al* [3, 4] performed extensive conceptual design studies to assess the benefits of variable-span wings in enhancing aerodynamic efficiency when actuated symmetrically and in improving roll control authority when actuated asymmetrically. The idea of span morphing is not new. Ivan Makhonine developed one of the earliest span morphing wing designs. The MAK-10 was an aircraft that flew in the 1930s with a telescopic span morphing wing. He used pneumatic actuators to morph the telescopic wing and his design was capable of achieving up to 60% span extension [5]. In recent years, there has been some promising work on span morphing wings. For example, Blondeau *et al* [6] developed a telescopic wing and they used hollow fibreglass shells to preserve the aerofoil shape and reduce the storage size of the wing. To reduce the weight, they used inflatable actuators instead of rigid spars to support the aerodynamic loads on the wing. Bae *et al* [7] conducted static and dynamic studies on the wing of a long-range cruise missile and identified some of the difficulties associated with the design of a morphing wing capable of span change. Their studies concluded a drag reduction of 25% and a range increase of 30% was possible. Ajaj *et al* [8–10] developed a number of wing designs that facilities changing the span. These designs include the Zigzag Wingbox concept [8], the Compliant Spar concept [9], and the Gear driveN Autonomous Twin Spar (GNATSpar) [10]. Most of the concepts developed by Ajaj *et al* [8–10] used a hybrid structural design philosophy where the wing structure is at the same time the mechanism and the actuator. The structure was then covered by flexible material (mainly elastomeric) to provide and maintain the aerodynamic profile. Similarly, Woods and Friswell [11] developed a hybrid span morphing design named the adaptive aspect ratio (AdAR) wing that utilises sliding ribs supporting an elastomeric skin. A more extensive review on span morphing technology (applications and concepts) for both fixed-wing and rotary-wing aircraft is given in Barbarino *et al* [1].

Recently, a number of research articles presented methods to study the aeroelastic behaviour of span morphing wings. For example, Huang and Qiu [12] developed a novel first-order state-space aeroelastic model based on Euler–Bernoulli beam theory (with time-dependent boundary conditions coupled with a reduced-order unsteady vortex lattice method). The morphing parameters, i.e., wing span length and morphing speed, are of particular interest for understanding the fundamental aeroelastic behaviour of variable-span wings. They concluded that faster span morphing results in a superior aeroelastic performance but increase the complexity of the mechanism. Similarly, Li and Jin [13] studied the dynamical behaviour and stability of a variable-span wing subjected to supersonic aerodynamic loads. They modelled the span morphing wing as an axially moving cantilever plate and established the governing equations of motion using Kane's method and piston theory. They concluded that a periodically varying (with proper amplitude) morphing law can facilitate flutter suppression.

This paper studies the impact of span morphing on the aeroelastic behaviour of uniform cantilever wings. It assesses the feasibility of utilising span morphing technology as an active flutter suppression device to expand the flight envelopes of aircraft. To accomplish these aims/objectives, a low-fidelity, aeroelastic model will be developed according to the Rayleigh–Ritz method to represent the wing structure using bending and torsion shape functions and Theodorsen's aerodynamic theory will be used to quantify the unsteady aerodynamic loads acting on the wing. The outcomes of this study are essential to the design of a robust control law similar to the flight control analysis conducted by Oktay and Sultan [14].

2. Aeroelastic model

2.1. Two degrees of freedom dynamic model

In order to assess the pure impact of span morphing on the aeroelastic behaviour of wings, rectangular, uniform, cantilever wings are chosen to minimise the interference and influence from other geometric (taper) and aeroelastic couplings (sweep). This model assumes a clean span morphing wing configuration where no control surfaces or engines are attached to it and there are no fuel tanks embedded within the wing. The continuous, multi-degrees of freedom, wing structure is modelled as a two degrees of freedom system via the Rayleigh–Ritz method using shape functions. These shape functions correspond to the uncoupled first bending and first torsional modes of a uniform cantilever beam. The first bending mode shape function, $h(y)$, is given as:

$$h(y) = 0.5[(\cosh(B_n y) - \cos(B_n y)) - \sigma_n(\sinh(B_n y) - \sin(B_n y))], \quad (1)$$

where y is the spanwise position measured from the wing root and

$$\sigma_n = \frac{(\cosh(B_n l) + \cos(B_n l))}{(\sinh(B_n l) + \sin(B_n l))} \quad (2)$$

and

$$B_n l = 1.875, \quad (3)$$

where l is the wing semi-span. The torsion shape function, $\phi(y)$, is given as

$$\phi(y) = \sin\left(\frac{\pi}{2l}y\right). \quad (4)$$

This allows the wing to be modelled as an equivalent two degrees of freedom aerofoil whose generalised coordinates are defined at the wingtip. Using the shape functions, the plunge displacement, speed and acceleration at any spanwise location (y) can now be related to those of the wingtip (generalised coordinates) as

$$\begin{aligned} w(t, y) &= w_t(t)h(y) \\ \dot{w}(t, y) &= \dot{w}_t(t)h(y) \\ \ddot{w}(t, y) &= \ddot{w}_t(t)h(y). \end{aligned} \tag{5}$$

Similarly, the pitch displacement, speed and acceleration at any spanwise location (y) can now be related to those of the wingtip (generalised coordinates) as

$$\begin{aligned} \theta(t, y) &= \theta_t(t)\,\phi(y) \\ \dot{\theta}(t, y) &= \dot{\theta}_t(t)\,\phi(y) \\ \ddot{\theta}(t, y) &= \ddot{\theta}_t(t)\,\phi(y), \end{aligned} \tag{6}$$

where $w_t(t)$ and $\theta_t(t)$ represent the generalised coordinates coinciding with the wingtip. It should be noted that the datum from which the generalised coordinates are measured is the static position of the wingtip when the wing deflects due to its self-weight only. In fact, during span morphing, parameters such as overall mass and mass moment of inertia of the wing and their spanwise distributions, the torsional rigidity, and bending rigidity may vary. The way they vary depends mainly on the span morphing concept and the actuation mechanism used. For instance, in a telescopic mechanism consisting of overlapping wing sections as the wing span varies, the mass per unit span will change. In addition, the ratio of y/l is not constant with telescopic concepts and hence the above shape functions are time-dependent and equations (5) and (6) are not correct. On the other hand, some recent morphing concepts uses a hybrid structural layout where an internal mechanism is covered by flexible skin. Usually for most of these hybrid concepts the bending and torsion shape functions are time independent because the ratio of y/l remains constant during and after morphing if these concepts are employed across the entire wing span. Therefore, the focus of this paper will be on these hybrid span morphing concepts where y/l remains constant. Some good examples of these concepts are the Zigzag Wingbox Concept [8], the Compliant Spar [9], and the GNATSpar [10]. Lagrange's equations of motions for a system with multiple degrees of freedom are expressed as

$$\frac{d}{dt}\left(\frac{\partial(T-U)}{\partial \dot{q}_i}\right) - \frac{\partial(T-U)}{\partial q_i} = Q_i, \tag{7}$$

where T is the total kinetic energy of the wing, and U is the total potential energy of the wing, q_i represents the ith generalised coordinate, $\dot{q}_i$ is the first-time derivative of the ith generalised coordinate, and Q_i is the ith applied force or moment. The total kinetic energy and total elastic potential

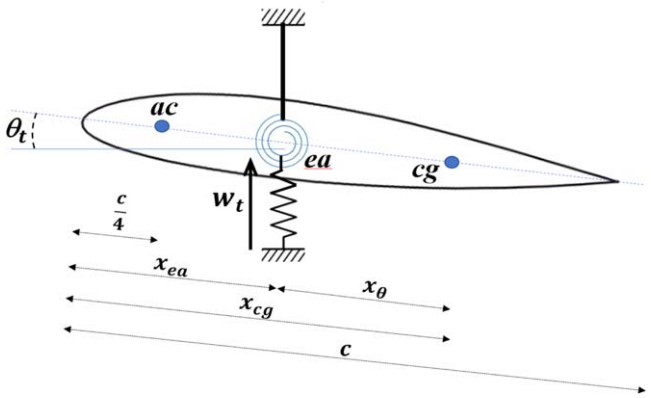

Figure 1. Two-dimensional representation of a uniform, cantilever, rectangular wing.

energy of the wing can be expressed as

$$\begin{aligned} T = \frac{1}{2}m'\dot{w}_t{}^2\int_0^l h^2 dy + \frac{1}{2}I'_{ea}\dot{\theta}_t{}^2\int_0^l \phi^2 dy \\ - m'x_\theta \dot{w}_t\dot{\theta}_t\int_0^l h\phi dy \end{aligned} \tag{8}$$

and

$$U = \frac{1}{2}\overline{GJ}\theta_t{}^2\int_0^l\left(\frac{d\phi}{dy}\right)^2 dy + \frac{1}{2}\overline{EI}w_t{}^2\int_0^l\left(\frac{d^2h}{dy^2}\right)^2 dy, \tag{9}$$

where m' is the mass per unit length, x_θ is the distance between the elastic axis (ea) and centre of gravity (cg) (defined as positive when cg is behind ea) as shown in figure 1. The integrals of the shape functions in the above equations can be simplified further as illustrated in table 1. It should be noted that structural damping is not considered in this study.

After integrating the shape functions, the equations for total kinetic and potential energies become

$$T = \frac{1}{8}m'l\dot{w}_t{}^2 + \frac{1}{4}I'_{ea}l\dot{\theta}_t{}^2 - 0.3389m'lx_\theta\dot{w}_t\dot{\theta}_t \tag{10}$$

and

$$U = \frac{\pi^2}{16l}\overline{GJ}\theta_t{}^2 + \frac{3.09}{2l^3}\overline{EI}w_t{}^2. \tag{11}$$

The full equations of motion of the equivalent two-dimensional model (including the span morphing dynamic terms) are developed using Lagrangian mechanics. The equations of motion relative to w_t and θ_t respectively can be expressed as:

$$\begin{aligned} \frac{1}{4}m'l\ddot{w}_t + \frac{1}{4}m'\dot{l}\dot{w}_t + \frac{1}{4}\dot{m}'l\dot{w}_t - 0.3389m'lx_\theta\ddot{\theta}_t \\ - 0.3389m'\dot{l}x_\theta\dot{\theta}_t - 0.3389\dot{m}'lx_\theta\dot{\theta}_t + \frac{3.0901}{l^3}\overline{EI}w_t = L \end{aligned} \tag{12}$$

Table 1. Shape functions.

Bending shape function	$\int_l^0 h^2 dy = \frac{l}{4}$	$\int_l^0 \left(\frac{d^2h}{dy^2}\right)^2 dy = \frac{3.09}{l^3}$	$\int_l^0 h\phi dy = 0.3389l$
Torsion shape function	$\int_0^l \phi^2 dy = \frac{l}{2}$	$\int_0^l \left(\frac{d\phi}{dy}\right)^2 dy = \frac{\pi^2}{8l}$	

and

$$\frac{1}{2}m'lr_\theta^2\ddot{\theta}_t + \frac{1}{2}m'\dot{l}r_\theta^2\dot{\theta}_t + \frac{1}{2}\dot{m}'lr_\theta^2\dot{\theta}_t - 0.3389m'lx_\theta\ddot{w}_t - 0.3389m'\dot{l}x_\theta\dot{w}_t - 0.3389\dot{m}'lx_\theta\dot{w}_t + \frac{\pi^2}{8l}\overline{GJ}\theta_t = M_{ea}. \tag{13}$$

It should be noted that r_θ is the radius of gyration, I'_{ea} is mass moment of inertia per unit span around ea and it can be expressed as $I'_{ea} = m'r_\theta{}^2$. Furthermore, $\overline{GJ}$ is the torsional rigidity, $\overline{EI}$ is the bending rigidity, L is the equivalent lift force acting on the equivalent aerofoil, and M_{ea} is the equivalent pitching moment acting on the elastic axis of the equivalent aerofoil. The total equivalent lift force and pitching moment around the elastic axis can be obtained as:

$$L = \int_0^l L'h(y)dy \tag{14}$$

and

$$M_{ea} = \int_0^l M'_{ea}\,\phi(y)\,dy, \tag{15}$$

where L' is the unsteady lift per unit span and M'_{ea} is the unsteady pitching moment around the elastic axis per unit span.

2.2. Aerodynamic model

Theodorsen's unsteady aerodynamic theory, developed in 1935, is used to model the aerodynamic forces and moments acting on the wing. Theodorsen's unsteady aerodynamics model has a circulatory component to account for the effect of the wake on the aerofoil and it contains the main damping and stiffness terms and a non-circulatory component to account for the acceleration of the fluid surrounding the aerofoil [15]. The work of Theodorsen is based on the following assumptions:

- Thin aerofoil;
- potential, incompressible flow;
- the flow remains attached, i.e. the amplitude of oscillations is small; and
- the wake behind the aerofoil is flat.

According to Theodorsen's unsteady aerodynamic theory, L' and M'_{ea} can be expressed respectively as

$$L' = \pi\rho\frac{c^2}{4}\left[-\ddot{w} + V\dot{\theta} - \hat{a}\frac{c}{2}\ddot{\theta}\right] + 2\pi\rho V\frac{c}{2}C(k) \times \left[-\dot{w} + V\theta + \frac{c}{2}\left(\frac{1}{2} - \hat{a}\right)\dot{\theta}\right] \tag{16}$$

and

$$M'_{ea} = L'\left[\frac{c}{4} + \frac{\hat{a}c}{2}\right] + \pi\rho\frac{c^3}{8}\left[\frac{\ddot{w}}{2} - V\dot{\theta} - \frac{c}{2}\left(\frac{1}{8} - \frac{\hat{a}}{2}\right)\ddot{\theta}\right], \tag{17}$$

where ρ is the air density, c is the chord of the wing at any location (uniform across the span), $\hat{a} = \frac{2x_{ea}}{c} - 1$ is the normalised pitch axis location with respect to half chord, and $C(k)$ is the frequency-dependent, Theodorsen's transfer function that accounts for attenuation of lift amplitude and phase lag in lift response due to sinusoidal motion, in this paper, a low-dimensional state-space representation of the classical unsteady aerodynamic model of Theodorsen developed by Brunton and Rowley [16] was employed. They used a Padé approximation for Theodorsen's transfer function which was used to develop reduced-order models for the effect of synthetic jet actuators on the forces and moments on an aerofoil [16, 17]. The approximate transfer function $C(s)$ in the Laplace domain becomes

$$C(s) \approx \frac{0.5177a^2s^2 + 0.2752as + 0.01576}{a^2s^2 + 0.3414as + 0.01582}, \tag{18}$$

where

$$a = \frac{c}{2V}. \tag{19}$$

The equivalent lift force becomes

$$L = \frac{0.0985}{a}\dot{u} + \frac{0.0076}{a^2}u + 0.5177\hat{B}V\theta_t\int_0^l h\phi dy + \left(0.5177\hat{B}\frac{c}{2}\left(\frac{1}{2} - \hat{a}\right) + \hat{A}V\right)\dot{\theta}_t\int_0^l h\phi dy - \hat{A}\left(\frac{\hat{a}c}{2}\right)\ddot{\theta}_t\int_0^l h\phi dy - 0.5177\hat{B}\dot{w}_t\int_0^l h^2dy - \hat{A}\ddot{w}_t\int_0^l h^2dy, \tag{20}$$

where

$$\ddot{u} = -\frac{0.3414}{a}\dot{u} - \frac{0.0158}{a^2}u - \hat{B}\dot{w}_t\int_0^l h^2dy + \hat{B}\left[V\theta_t + \frac{c}{2}\left(\frac{1}{2} - \hat{a}\right)\dot{\theta}_t\right]\int_0^l h\phi dy \tag{21}$$

while

$$\hat{A} = \pi\rho\frac{c^2}{4} \tag{22}$$

and

$$\hat{B} = 2\pi\rho V\frac{c}{2}. \tag{23}$$

Similarly, the equivalent pitching moment becomes

$$M_{ea} = \frac{0.0985}{a}\frac{c}{2}\left(\frac{1}{2}+\hat{a}\right)\dot{v} + \frac{0.0076}{a^2}\frac{c}{2}\left(\frac{1}{2}+\hat{a}\right)v + 0.5177\frac{c}{2}\left(\frac{1}{2}+\hat{a}\right)\hat{B}V\theta_t\int_0^l \phi^2 dy + \left(\frac{0.5177\hat{B}c^2}{4}\left(\frac{1}{2}-\hat{a}\right)\left(\frac{1}{2}+\hat{a}\right) + \hat{A}V\frac{c}{2}\left(\frac{1}{2}+\hat{a}\right) - \hat{A}V\frac{c}{2}\right)\dot{\theta}_t\int_0^l \phi^2 dy - \frac{\hat{A}c}{2}\left(\frac{c}{2}\left(\frac{1}{8}-\frac{\hat{a}}{2}\right)+\left(\frac{1}{2}+\hat{a}\right)\left(\frac{\hat{a}c}{2}\right)\right)\ddot{\theta}_t\int_0^l \phi^2 dy - 0.5177\frac{c}{2}\left(\frac{1}{2}+\hat{a}\right)\hat{B}\dot{w}_t\int_0^l h\phi dy - \hat{A}\frac{c}{2}\left(\left(\frac{1}{2}+\hat{a}\right)-\frac{1}{2}\right)\ddot{w}_t\int_0^l h\phi dy, \quad (24)$$

where

$$\ddot{v} = -\frac{0.3414}{a}\dot{v} - \frac{0.0158}{a^2}v - \hat{B}\dot{w}_t\int_0^l h\phi dy + \hat{B}\left[V\theta_t + \frac{c}{2}\left(\frac{1}{2}-\hat{a}\right)\dot{\theta}_t\right]\int_0^l \phi^2 dy. \quad (25)$$

2.3. Validation

The aeroelastic model developed here is validated against other exiting models through predicting the flutter speed, frequency and divergence speed for the Goland wing, the wing of a high altitude long endurance (HALE) aircraft, and a representative rectangular wing described in table 2.

It is essential to determine whether the binary aeroelastic model (first bending and first torsion modes only) developed here is sufficiently accurately to predict the flutter speed and frequency for uniform cantilever wings at various span extensions. Therefore, the binary aeroelastic model is compared with a multimode aeroelastic model that considers the first 6 modes (1st 3 bending modes and 1st 3 torsional modes). The multimode aeroelastic model is based on the same assumptions as the binary aeroelastic model but it takes into account higher number of vibrational modes. The flutter

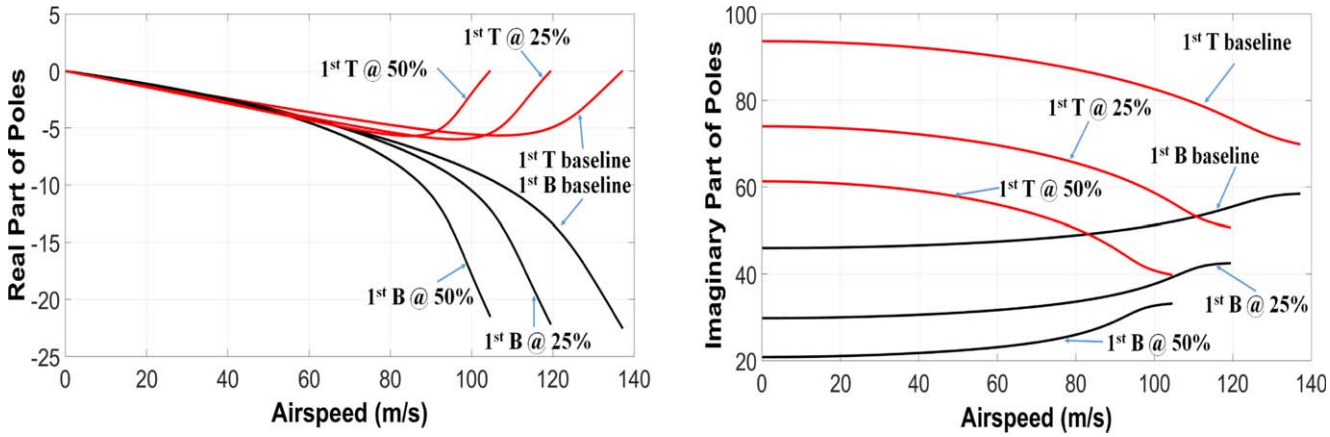

a. Real part of poles **b. Imaginary part of poles**

Figure 2. Binary flutter modes of Goland wing at different span extensions (baseline, 25% and 50%).

Table 2. Properties of representative wings used for validation.

Specifications	HALE wing	Goland wing	Representative wing
Half span (m)	16	6.096	3
Chord (m)	1	1.8288	1
Mass per unit length (kg m^{-1})	0.75	35.71	6
Moment of inertia (50% chord) (kg m)	0.1	8.64	0.75
Spanwise elastic axis (from LE)	50%	33%	35%
Centre of gravity (from LE)	50%	43%	45%
Spanwise bending rigidity (N m^2)	2×10^4	9.77×10^6	6×10^5
Torsional rigidity (N m^2)	1×10^4	0.987×10^6	6×10^4
Chordwise bending rigidity (N m^2)	4×10^6	—	—
Density of air kg m^{-3}	0.0889	1.225	1.225

Table 3. Validation study.

	Method						
Wing	Present work binary	Present work (first 6 modes)	Reference [18]	Reference [19]	Reference [20]	Reference [21]	Reference [12]
HALE Wing							
Flutter speed ($m\,s^{-1}$)	33.43	33.25	32.21	—		32.51	—
Flutter freq ($rad\,s^{-1}$)	21.38	21.54	22.61	—		22.37	—
Divergence speed ($m\,s^{-1}$)	37.18	37.18	37.29	—		37.15	—
Goland Wing							
Flutter speed ($m\,s^{-1}$)	137.11	135.9	—	135.6	136.22	137.16	133
Flutter freq ($rad\,s^{-1}$)	69.9	70.4	—	70.2	70.06	70.7	72.7
Divergence speed ($m\,s^{-1}$)	252.8	252.8	—	—	250.82	—	—
Representative Wing							
Flutter speed ($m\,s^{-1}$)	78.33	76.36	—	—		—	77
Flutter freq ($rad\,s^{-1}$)	148.94	149.66	—	—		—	149.6
Divergence speed ($m\,s^{-1}$)	206.70	206.70	—	—		—	—

speed and frequency from the 2 aeroelastic models (binary and multimode) for each of the wings listed in table 2 are presented in table 3.

It is evident from table 3, that the binary aeroelastic model predicts the flutter speed and frequency accurately enough and considering higher aeroelastic modes has minor effect on the results. Furthermore, a comparison between the binary aeroelastic model and the multimode aeroelastic model is performed using Goland wing at 3 different span extensions.

Figure 2 shows the variation of the aeroelastic modes (1st bending and 1st torsion only) with at different span extensions (0%, 25% and 50%) for Goland wing using the binary aeroelastic model. It is evident that for the different span extensions considered, the 1st torsion mode is the one that flutters. At flutter, the imaginary parts (frequencies) of the two modes get close but do not coalesce. As the wing span is increased, the frequencies of the two modes at flutter get very close but still do not coalesce. As the airspeed increases from zero up to the flutter speed, the frequency of the torsion mode drops while that of the bending mode increases. On the other hand, the real part of the poles representation the 1st torsion mode increases (negatively) indicating an increase in the damping of this mode until a critical airspeed is reached after which the real part reduces and get to zero at the flutter speed.

Figure 3 shows the variation of the aeroelastic modes (1st bending, 2nd bending, 3rd bending, 1st torsion, 2nd torsion and 3rd torsion) with different span extensions (0%, 25% and 50%) for Goland wing using the multimode aeroelastic model. The 3rd torsion is considered but not plotted because the real and imaginary parts of the corresponding poles are very large. It can be seen from figure 3, that the 1st bending and 1st torsion are the dominant flutter modes regardless of span extension for this uniform cantilever wing. This verify that the binary aeroelastic model developed here is sufficient and accurate enough for the purpose of this study.

Following the validation process using Goland, HALE, and representative wings, the binary aeroelastic model is utilised to study flutter of span morphing wings and assess the feasibility of span morphing as an active flutter suppression device. It should be noted that in all the figures presented below, the flutter speed is normalised by the flutter speed of the baseline (non-morphing) wing (either Goland or HALE) at the flight conditions described in table 2. The same applies for flutter frequency and divergence speed.

3. Variation of flutter speed

3.1. Flutter versus span extension

It is well known that flutter speed and frequency are very sensitive to wing span. To understand the impact of wing span (without taking into account the morphing rate) on flutter speed and frequency, the span of the HALE's wing was varied quasi-statically while keeping m' and I'_{ea} constants. Such an assumption is true for the GNATSpar concept where the spars of the wing are larger than the baseline wing span and the extra length of these spars is stored in the fuselage and opposite sides of the wing. As the wing span varies, the mass per unit span, radius of gyration, torsional rigidity and bending rigidity all remain constant. For more details on the GNATSpar Concept, the reader is advised to see Ajaj *et al* [10]. Figure 4 shows the variation of flutter speed, frequency and divergence speed with span extension for the HALE GNATSpar wing. It is obvious that doubling the wing span reduces the flutter speed, flutter frequency and divergence speed by 50%. For a rectangular wing, flutter occurs before divergence and therefore it sets an upper limit on the maximum operating speed. The strong dependency of flutter on

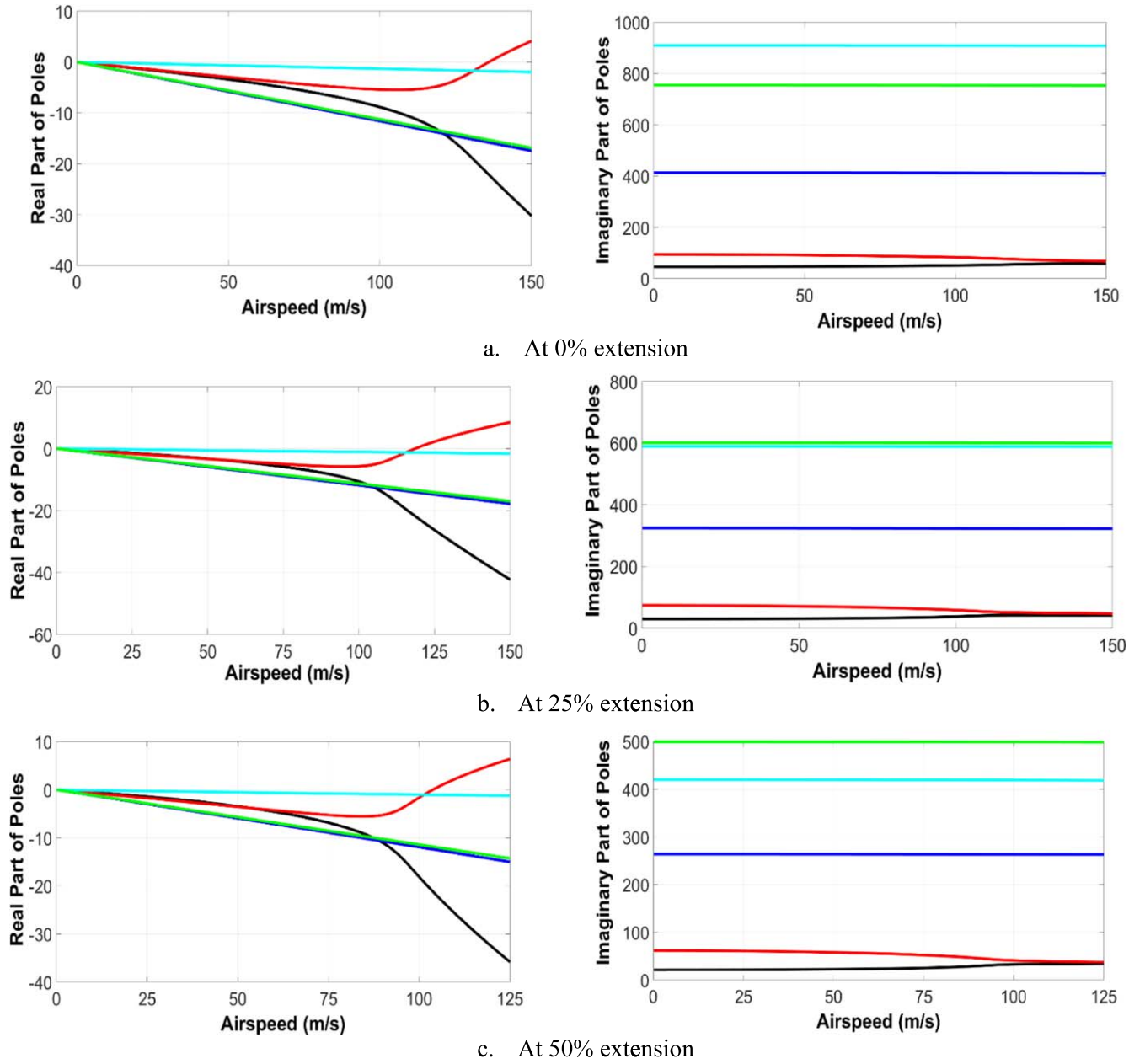

Figure 3. Flutter modes of Goland wing at different span extensions (Black for 1st bending, Red for 1st Torsion, Blue for 2nd Bending, Cyan for 2nd torsion, and Green for 3rd bending).

wing span implies that the span morphing technology can be used as a flutter suppression device widely expanding the operational margin of aircraft allowing one air vehicle to perform a range of missions effectively.

3.2. Flutter sensitivity to wing's parameters

For the GNATSpar wing, the mass per unit span, torsional rigidity and bending rigidity remain constant before, during and after extension as stressed above. However, there are a number of span morphing concepts where the mass per unit length, torsional rigidity, and bending rigidity varies as the wing extends or retracts. A good example of such concepts is the Zigzag Wingbox developed by the authors [8]. Although these changes in the wing mass and geometry properties can occur uniformly across the wing span, they will still have significant impact on the flutter speed and frequency and this must be account. This subsection presents the sensitivity of flutter speed and frequency of the Goland wing to these parameters. It is evident from figure 5 that the flutter speed and frequency are sensitive to mass per unit length. As the mass per unit span increases, the flutter speed and frequency drop irrespective of the wing span.

Figure 6 shows the variations of flutter speed, frequency and divergence speed with torsional rigidity at different wingspans. It can be deduced that flutter and divergence are very sensitive to torsional rigidity. As the wing span increases, the sensitivity of flutter speed to torsional rigidity increases. For very low torsional rigidity, flutter speed is almost independent of the wing span. As the torsional rigidity

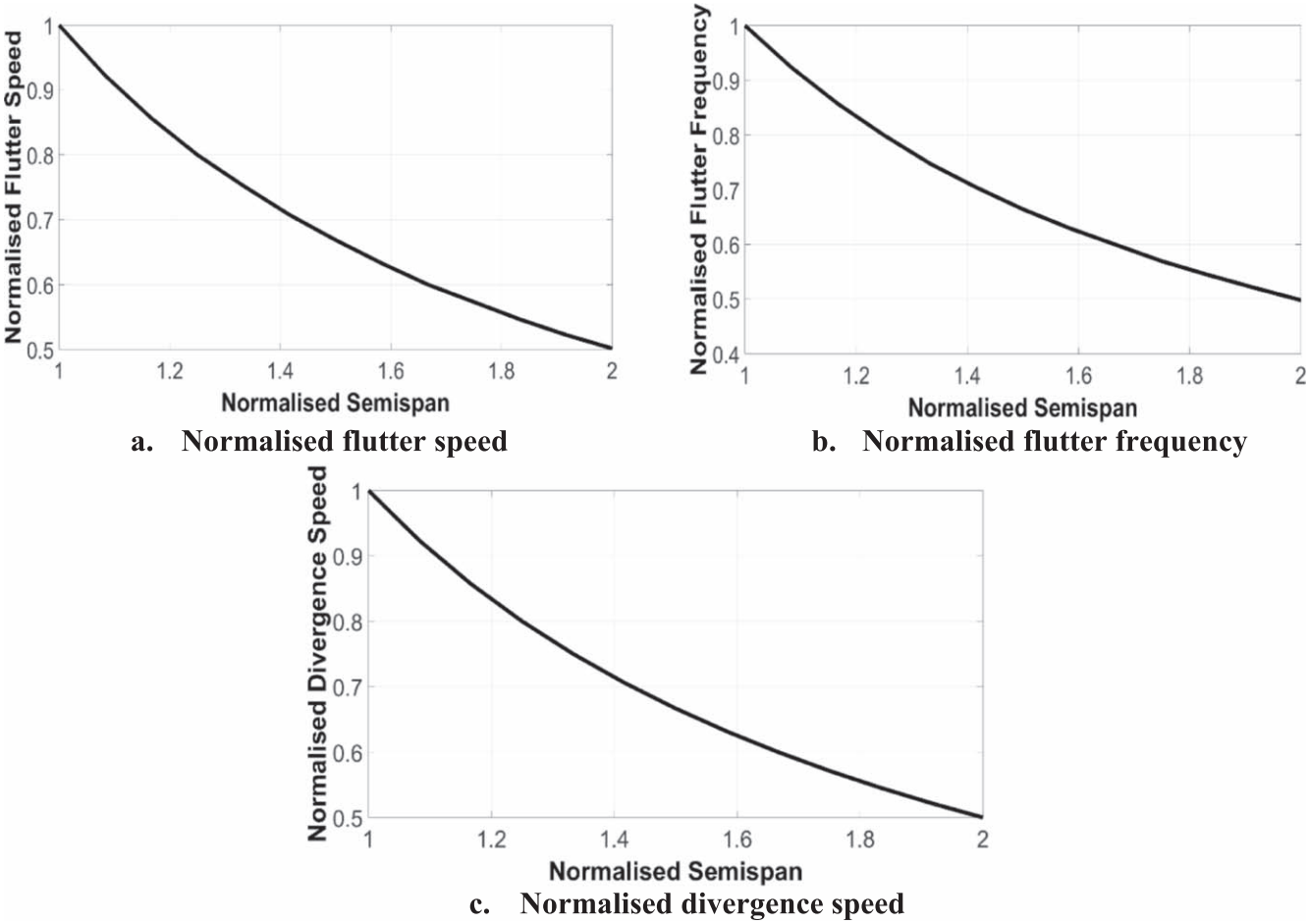

Figure 4. Variation aeroelasticity with span extension for the HALE wing.

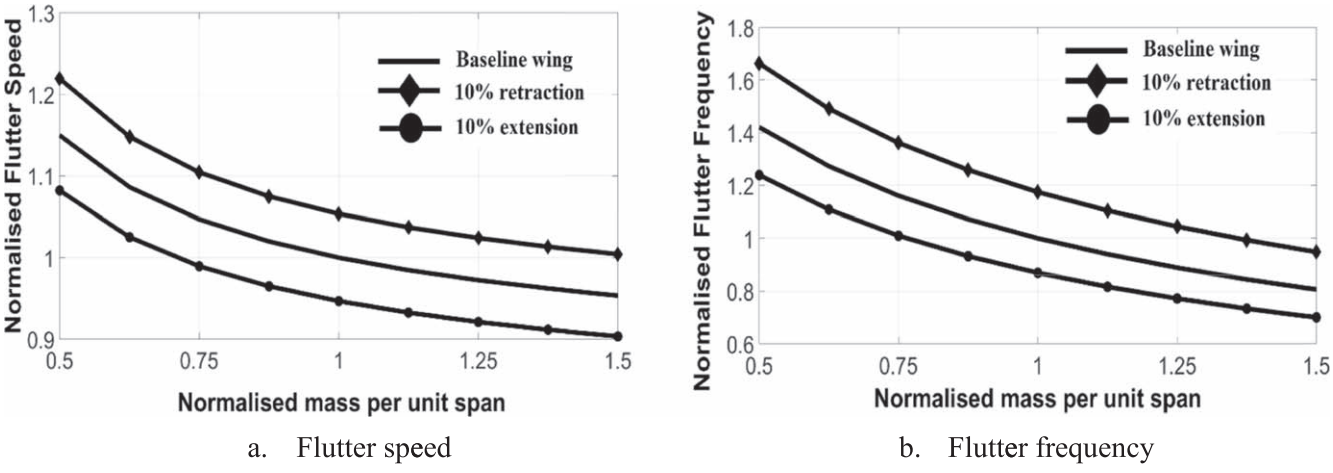

Figure 5. Variation of flutter with mass per unit span for Goland GNATSpar wing.

increases, the flutter speed, frequency and divergence speed increase making the wing less prone to static and dynamic aeroelastic phenomenon.

Figure 7 shows variation of flutter with bending rigidity. It can be clearly seen that as bending rigidity increases; the flutter speed reduces slightly while the flutter frequency increases. As the bending rigidity increases, the sensitivity of flutter speed to wing span reduces. The opposite is true for flutter frequency.

It should be noted that if the bending rigidity is increased further, the flutter speed further reduces until it reaches a critical point after which the flutter speed starts increasing again as shown in figure 8. This variation in the trend does not apply for torsional rigidity. Similarly, Fung [22] states that when bending rigidity is varied while keeping torsional

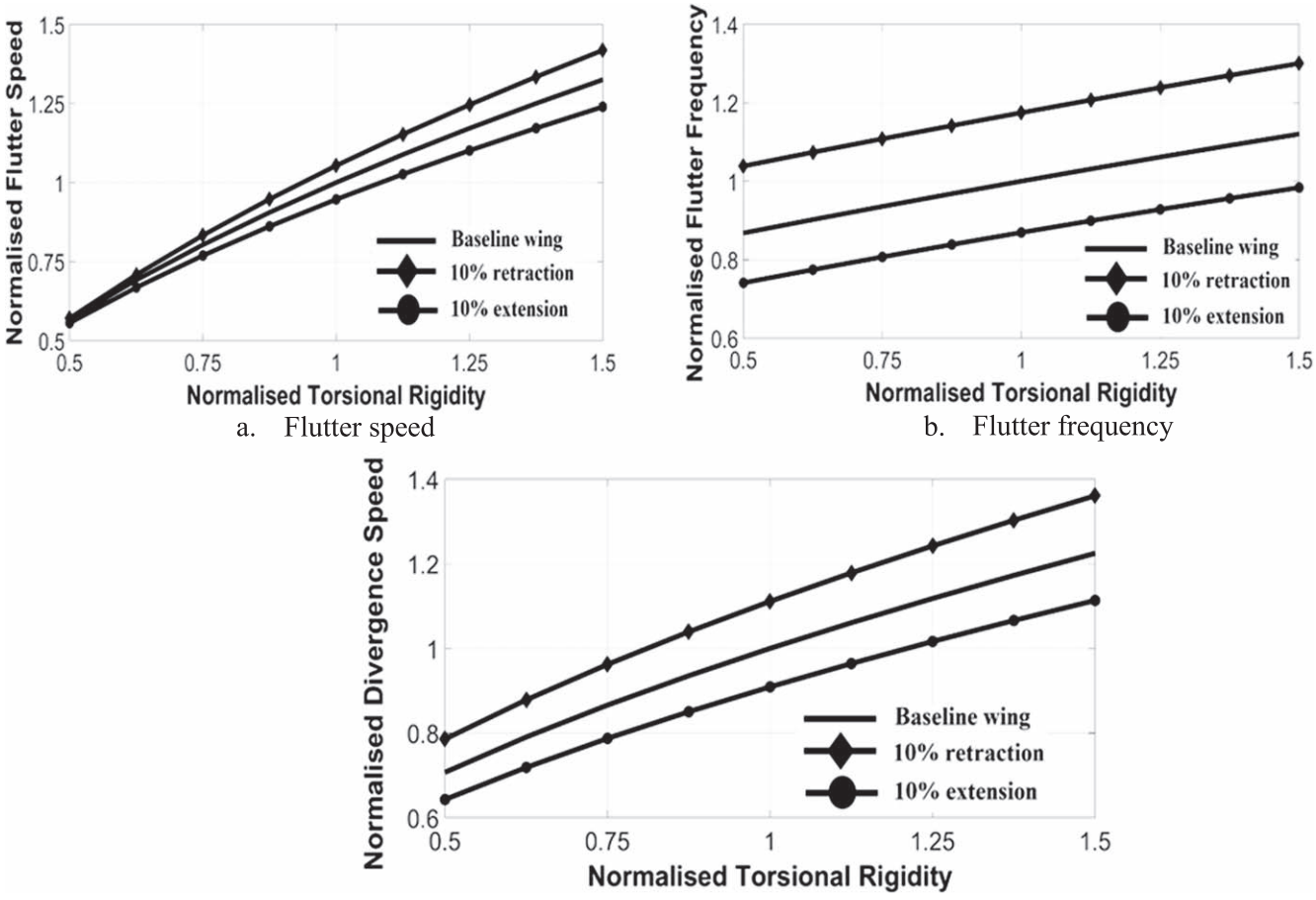

a. Flutter speed b. Flutter frequency

c. Divergence speed

Figure 6. Variation of flutter with torsional rigidity for Goland GNATSpar wing.

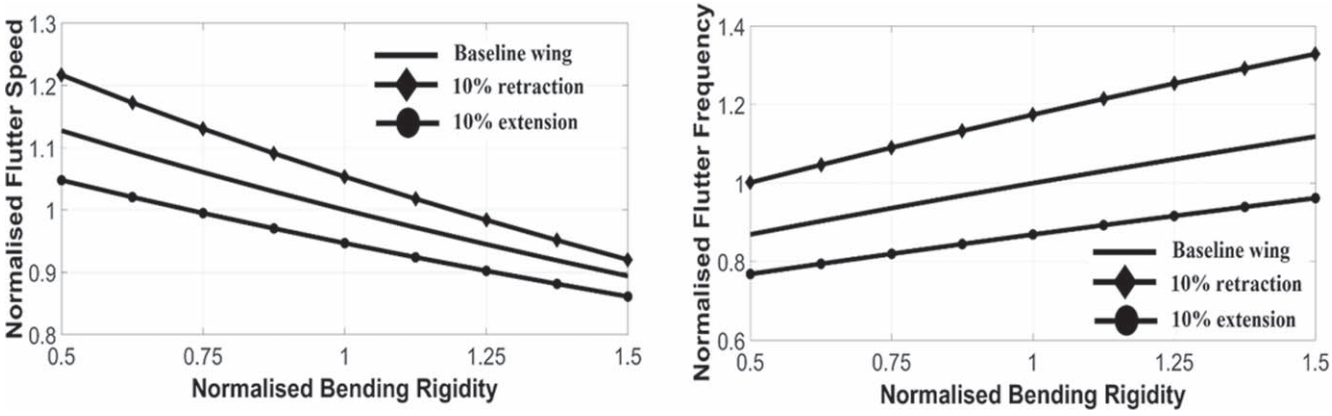

a. Flutter speed b. Flutter frequency

Figure 7. Variation of flutter with bending rigidity for Goland GNATSpar wing.

rigidity fixed, the flutter speed varies slightly but as the bending rigidity becomes very high the flutter speed reduces to a minimum. A further increase in the bending rigidity results in an increase in the flutter speed. Furthermore, it is evident that flutter speed and frequency are more sensitives to changes in torsional rigidity than to changes in bending rigidity.

3.3. Flutter versus morphing rate

It is anticipated from the dynamic equations derived above that the morphing rate (actuation speed) can affect the pitching and plunging motion of the wing and its flutter speed and frequency. In this analysis, the HALE wing described above is used. The mass per unit span is kept constant ($m' =$ constant and $m' = 0$) while the morphing rate is varied

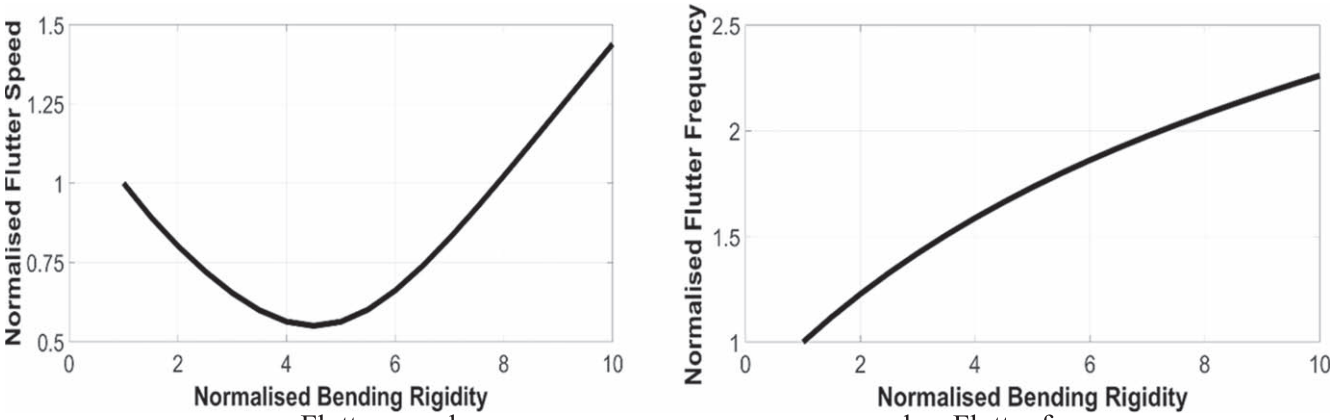

a. Flutter speed b. Flutter frequency

Figure 8. Variation of flutter speed with spanwise bending rigidity for Goland GNATSpar wing.

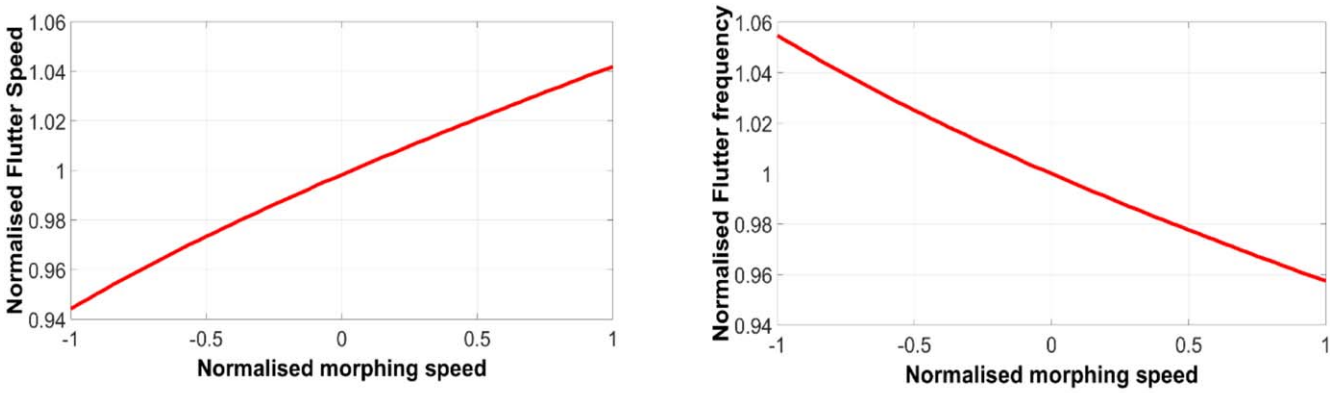

a. At baseline semispan.

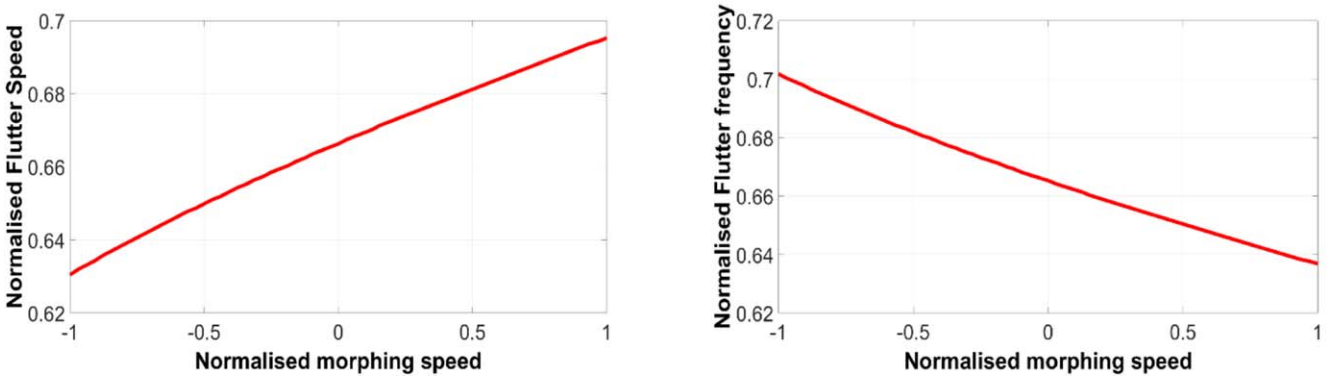

c. At 50% span extension.

Figure 9. Variation of flutter speed with morphing rate for the HALE wing.

from $-16\,\mathrm{m\,s^{-1}}$ (for retraction) to $+16\,\mathrm{m\,s^{-1}}$ (for extension). It should be noted that the $\pm 16\,\mathrm{m\,s^{-1}}$ is a hypothetical morphing rate and in practice the span morphing rate will be much smaller. This assumption is true for GNATSpar concept considered here. The bending and torsional rigidity are kept constant and uniform across the wing assuming they are not affected by morphing for the GNATSpar wing. The analysis is performed for two cases: the first case is when wing semi-span is at the baseline value (16 m) and the second case is when the wing semi-span is at 50% extension (24 m). Figure 9 shows the variation of flutter speed and frequency with the morphing rate and direction. It can be clearly seen that as the span extension rate increases, the flutter speed increases while the flutter frequency drops. On the other hand, as the span retraction rate increases, the flutter speed drops while the flutter frequency increases. This is consistent with the results of Huang and Qiu [12] who noticed an increase in the flutter speed as the extension rate increases and a decrease in the flutter speed as the retraction rate increases. It should be noted that in this analysis, the span morphing rate is assumed to be constant from the start till the end of the morphing process.

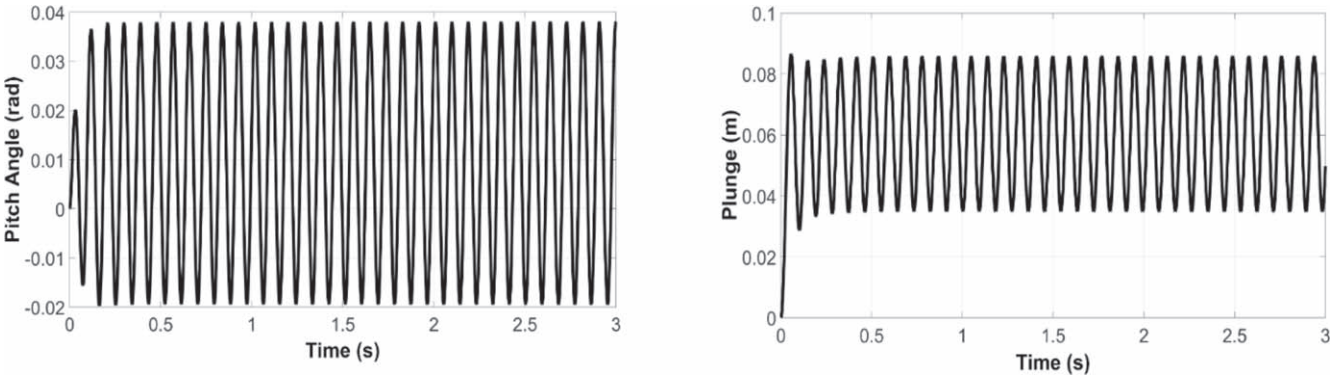

a. Wingtip pitch angle. b. Wingtip plunge.

Figure 10. Goland wing at the flutter speed (137.11 m s^{-1}) and 1° AOA (semi-span fixed at 6.096 m).

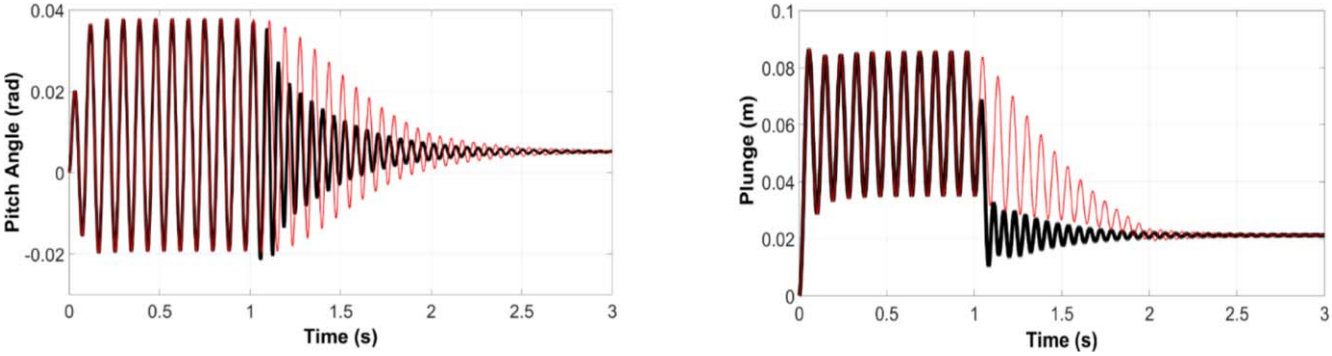

a. Wingtip pitch angle **b. Wingtip plunge**

Figure 11. Goland wing at the flutter speed (137.11 m s^{-1}) and 1° AOA. At $t = 1$ s, the semi-span is retracted by 20%. Two retraction speeds are considered (red thin curve for 1.2192 m s^{-1} and black thick curve for 12.192 m s^{-1}).

4. Flutter suppression

The aim of this section is to assess the feasibility of span morphing as an effective flutter suppression device. Span morphing technology is mainly integrated on an aircraft to facilitate multiple mission capability. For instance, the high aspect ratio is used to maximise endurance/range while the low aspect ratio is used to maximise manoeuvrability and agility. However, the span morphing technology, integrated for multi-mission capability, might also be used for flutter suppression, thus expanding the flight margin and allowing aircraft to operate at extreme speeds. To assess the feasibility of span morphing as an effective flutter suppression device, a number of representative scenarios are considered. In this analysis, the GNATSpar span morphing wing, whose mechanical and geometric properties are based on Goland wing, is employed. This implies that the mass per unit span, radius of gyration, torsional rigidity and bending rigidity all remain constants during and after span morphing [10]. The response time histories presented in the following subsections are obtained through solving the aeroelastic equations numerically using ODE23s in Matlab.

4.1. Scenario 1: fixed span at flutter speed

In this scenario, the wing is set at a 1° angle of attack and a speed of 137.11 m s^{-1} (which is the flutter speed of the wing). The wingtip oscillations in pitch and plunge as shown in figure 10. It can be clearly seen from figure 10 that when operating at the flutter speed the wing undergoes undamped oscillation in pitch and plunge. It should be noted that increasing the airspeed above the flutter speed will cause the wing oscillations to grow and diverge.

4.2. Scenario 2: span retraction at flutter speed

To investigate flutter suppression capability of span morphing, the span morphing of the Goland wing is set at 1° angle of attack and airspeed of 137.11 m s^{-1} (flutter speed of the baseline wing). The wing starts its undamped oscillation in pitch and plunge. After one second ($t = 1$ s), the wing span is retracted by 20%. Two actuation speeds are employed (1.2192 and 12.192 m s^{-1}). The behaviour of the wing for the different retraction speed can be seen in figure 11.

Figure 11 shows that span retraction shifts a neutrally stable system into a definitely stable system. The high retraction rate results in faster decay of the wing oscillation and a significant reduction in the amplitude of the oscillations. Figure 10(b) shows that the plunge displacement during and after retraction reduces significant because the reduced wing span causes an increased bending stiffness, hence less displacement.

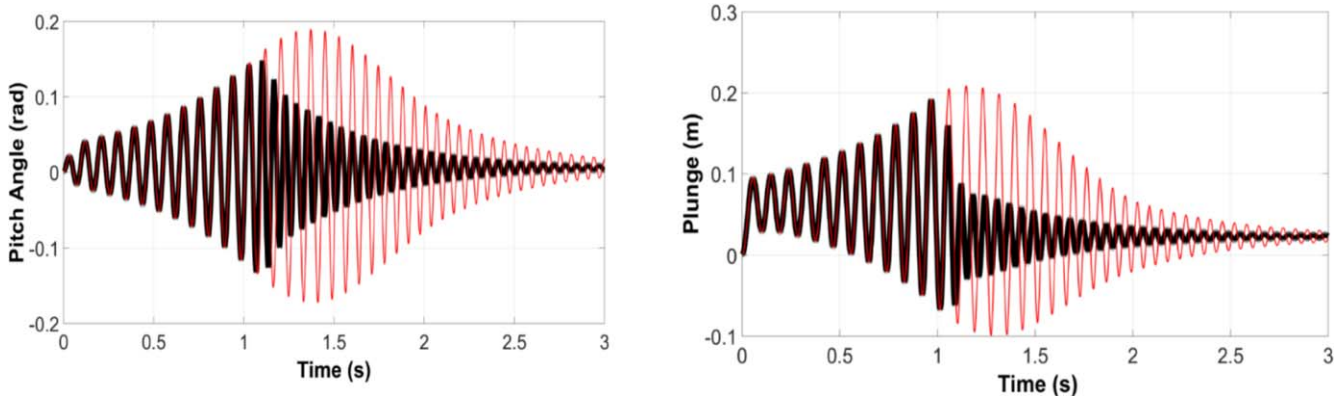

a. Wingtip pitch angle b. Wingtip plunge.

Figure 12. Goland wing at 142.11 m s^{-1} and 1° AOA. At $t = 1$ s, the semi-span is retracted by 20%. Two retraction speeds are considered (red thin curve for 1.2192 m s^{-1} and black thick curve for 12.192 m s^{-1}).

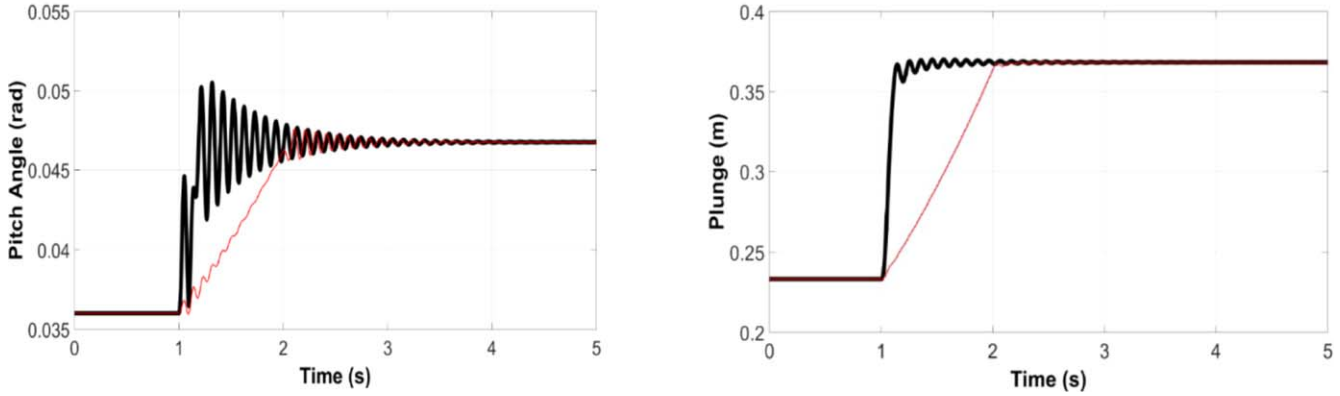

a. Wingtip pitch angle a. Wingtip plunge

Figure 13. Goland wing at 125 m s^{-1} and 5° AOA. At $t = 1$ s, the semi-span is extended by 10%. Two extension speeds are considered (red thin curve for 0.6096 m s^{-1} and black thick curve for 6.096 m s^{-1}).

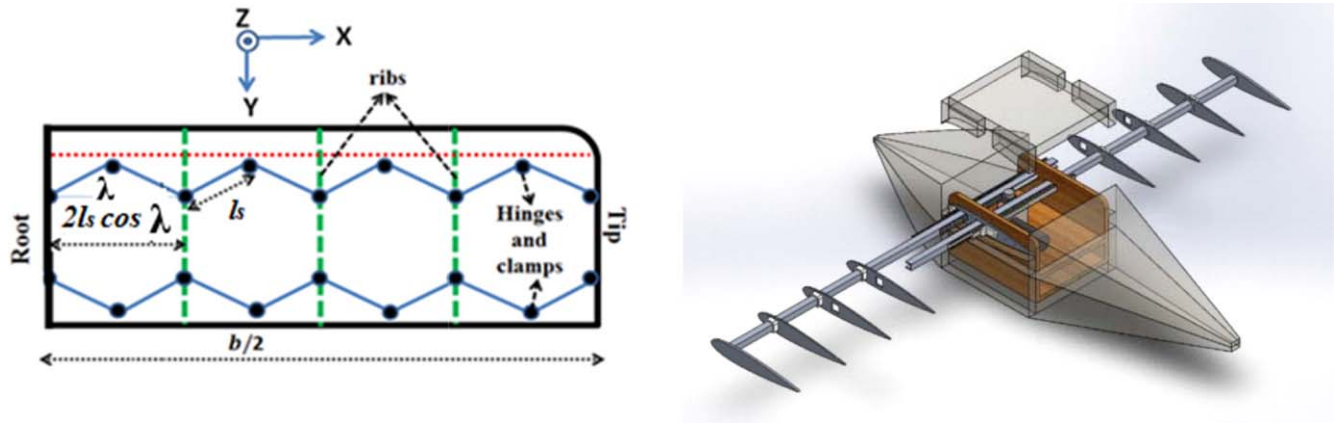

a. The Zigzag Wingbox [8]. b. The GNATSpar Wing [10].

Figure 14. Novel span morphing wings.

4.3. Scenario 3: span retraction above flutter speed

Another scenario is considered. The wing is set at 1° angle of attack and the airspeed is 142.11 m s^{-1} (5 m s^{-1} above the flutter speed). The wing oscillations start diverging. After 1 s, the wing span is retracted by 20%. Two actuation speeds are considered (1.2192 and 12.192 m s^{-1}). It is evident from figure 12 that span morphing can suppress flutter allowing the aircraft to operate over a wide range of airspeeds. As stated above, figure 12 also shows that the wingtip's oscillations damp out faster for higher span retraction rates. Span

morphing is capable of converting an unstable aeroelastic system into a strongly stable system.

4.4. Scenario 4: span extension below flutter speed

The span morphing Goland wing (at its baseline wing span) is set at 5° angle of attack at 125 m s^{-1} for some time (below the flutter speed). After the wing's oscillations settle, the wing semi-span (at $t = 1$ s) is extended by 10%. Two extension speeds were considered (0.6096 and 6.096 m s^{-1}). It is evident from figure 13 that extending the wing very fast results in high amplitude oscillations in pitch that take around 2 s to damp out. The oscillations in plunge are of much lower amplitude and damps out in around 1 s.

actuation to vary the wing span. The rotation of the beams in each partition with respect to the *Z*-axis (figure 14(a)) of the wing allows the span or length of the partition to be altered (extending or retracting depending on the direction of rotation). Each spar is also hinged at its two ends and attached to the adjacent ribs.

On the other hand, the GNATSpar concept is a wing whose spars are long than the original span of the wing [10]. The extra length of these spars is stored in the available space in the opposite sides of the wing and fuselage as shown in figure 14(b). The GNATSpar has a uniform cross-section spars along its wing span which is not possible with telescopic designs. The GNATSpar wing is actuated using a rack and a pinion mechanism that is part of the spar system. Both the Zigzag Wingbox and the GNATSpar wing are usually covered with fibre reinforced elastomeric skin supported by a Zero-Poisson's ratio honeycomb core.

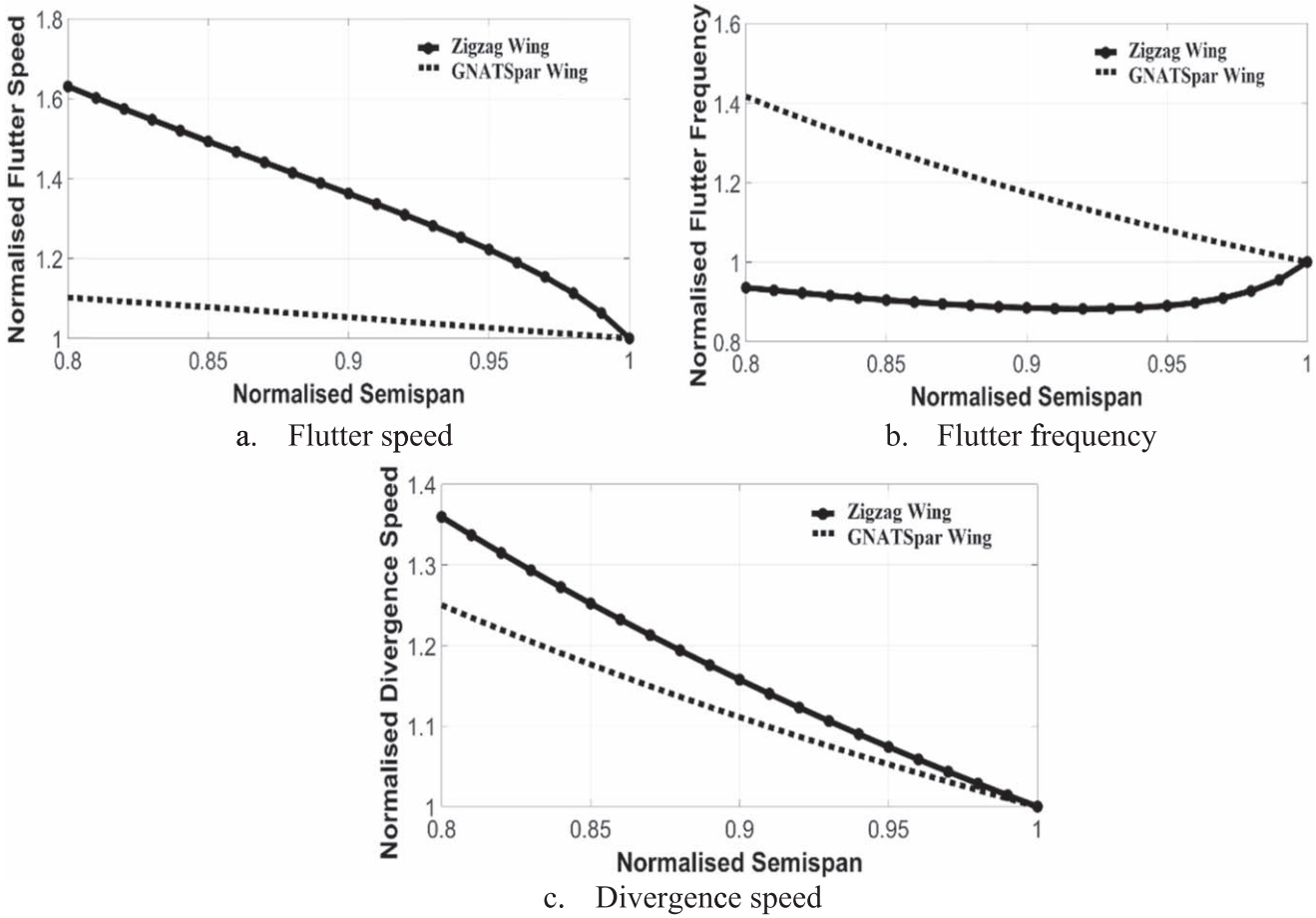

Figure 15. Variation of flutter for the Zigzag and GNATSpar mechanisms integrated into the Goland Wing.

5. Zigzag Wingbox versus GNATSpar wing

The Zigzag Wingbox is a span morphing concept developed by the authors [8]. It is a multi-partition wing where each partition consists of two spars located at the leading edge and trailing edge respectively. Each spar consists of two hinged beams and each beam has a box/rectangular cross-section. The angle between those two beams can be varied during

This section aims to compare the aeroelastic behaviour of both concepts. During this analysis, the influence of the skin and the core on the aerodynamic, mechanical and inertial properties of the wing will be ignored. For the Zigzag Wingbox, the mass per unit span (the wing mass remains constant), bending rigidity and torsional rigidity varies with wing span while they remain constant for the GNATSpar. To perform the comparison, each concept is separately integrated

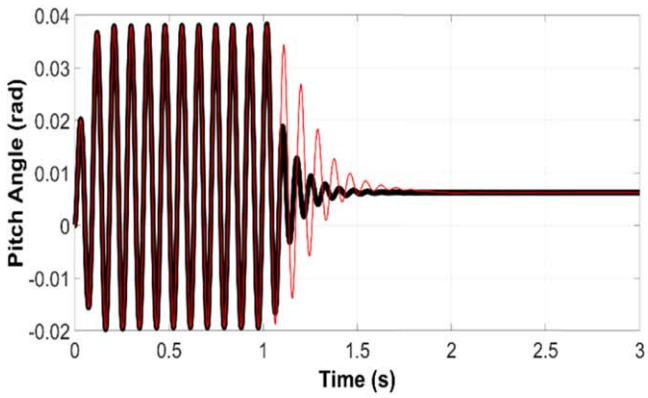

a. Wingtip pitch angle.

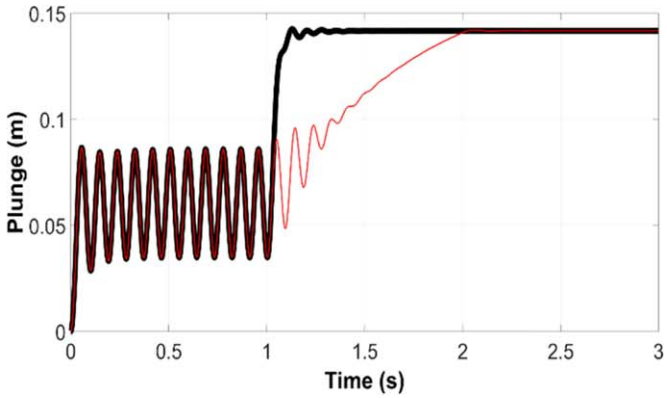

d. Wingtip plunge

Figure 16. Zigzag Goland wing at the flutter speed (137.11 m s^{-1}) and 1° AOA. At $t = 1$ s, the semi-span is retracted by 10%. Two retraction speeds are considered (red thin curve for 0.6096 m s^{-1} and black thick curve for 6.096 m s^{-1}).

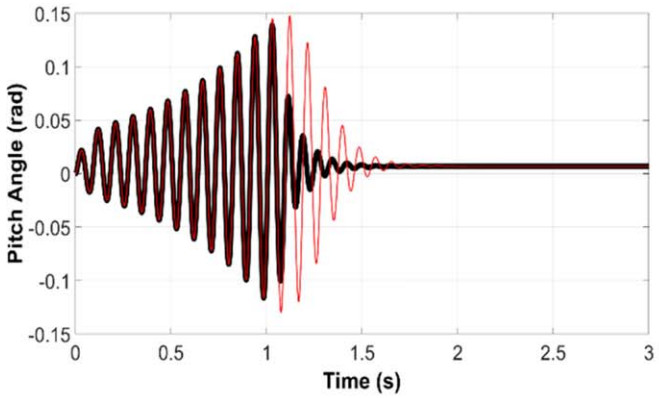

a. Wingtip pitch angle.

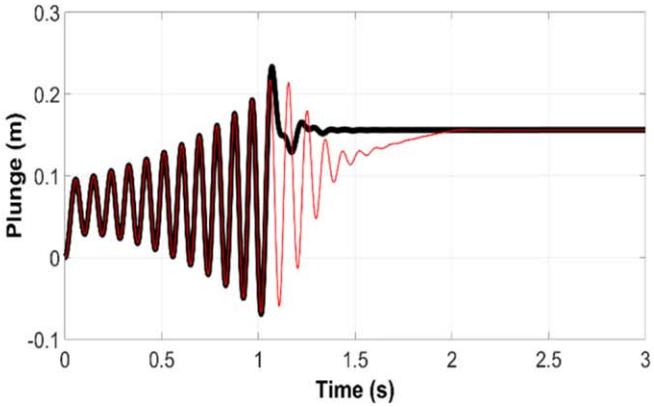

b. Wingtip plunge

Figure 17. Zigzag Goland wing at 142.11 m s^{-1} and 1° AOA. At $t = 1$ s, the semi-span is retracted by 10%. Two retraction speeds are considered (red thin curve for 0.6096 m s^{-1} and black thick curve for 6.096 m s^{-1}).

within the Goland wing. The mechanical and inertial properties of the Zigzag Wingbox are estimated using the appropriate formulas from Ajaj *et al* [8].

5.1. Quasi-static analysis

In this subsection, the wing span is varied quasi-statically and the wing geometric and mechanical properties are varied accordingly. The actuation rate and rate of change in mass per unit span are ignored. The flutter speed, frequency and divergence speed are computed accordingly. It should be noted that for the Zigzag Wingbox when the wing semi-span is equal to that of the baseline Goland wing (6.096 m), the angle ϕ is zero and its mass per unit length, torsional rigidity and bending rigidity match those of the baseline Goland wing (table 2). Therefore, only span retraction will be considered here. Figure 15 shows the variation of flutter speed, frequency and divergence speed for the two wings. It can be clearly seen that the behaviour of the GNATSpar is straight forward while the behaviour of the Zigzag Wingbox is more complex due to the severe changes in mass per unit length, torsional rigidity, and bending rigidity as the wing semi-span varies.

5.2. Dynamic analysis of the Zigzag Wingbox

In this subsection, the wing span of the Zigzag Wingbox is dynamically varied and the wing geometric and mechanical properties vary accordingly. Two retraction speeds are considered: 0.6096 and 6.096 m s^{-1}. The wing is set at a 1° angle of attack at 137.11 m s^{-1} (at the flutter speed). After one second ($t = 1$ s) the wing span is retracted by 10%. For the Zigzag Wingbox as the wing span reduces, the torsional rigidity increases while the bending rigidity reduces. This can be clearly seen in figure 16, where the reduction in wing span, stabilised the system but resulted in a much higher plunge displacement.

Following the above analysis, the wing is set at a 1° angle of attack and airspeed of 142.11 m s^{-1} (5 m s^{-1} above the flutter speed). The wing oscillations in pitch and plunge start diverging and at $t = 1$ s the wing span is reduced by 10%. Figure 17 shows that the reduction in wing span convert the system from being unstable to a one that is strongly stable. It should be noted that the plunge displacement is much higher.

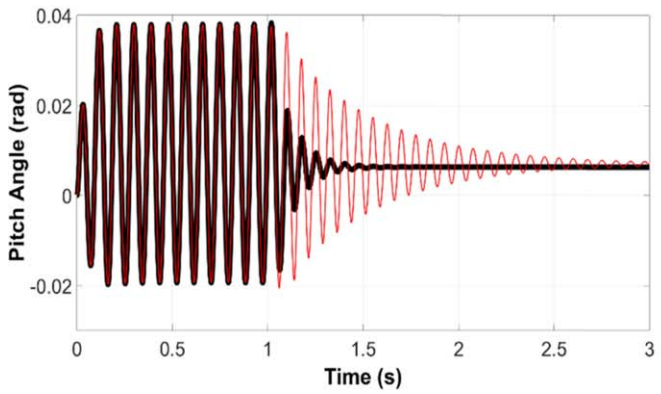

a. Wingtip pitch angle

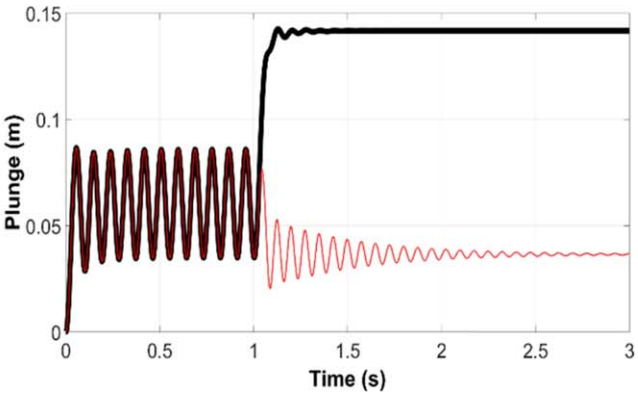

b. Wingtip plunge

Figure 18. Comparison between the Zigzag wingbox and the GNATSpar wing at 137.11 m s^{-1} and 1° AOA. At $t = 1$ s, the semi-span is retracted by 10% in 0.1 s (red thin curve for GNATSpar and black thick curve for Zigzag).

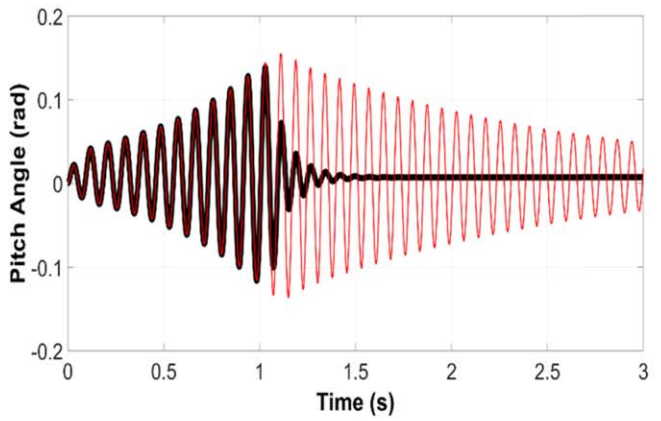

a. Wingtip pitch angle

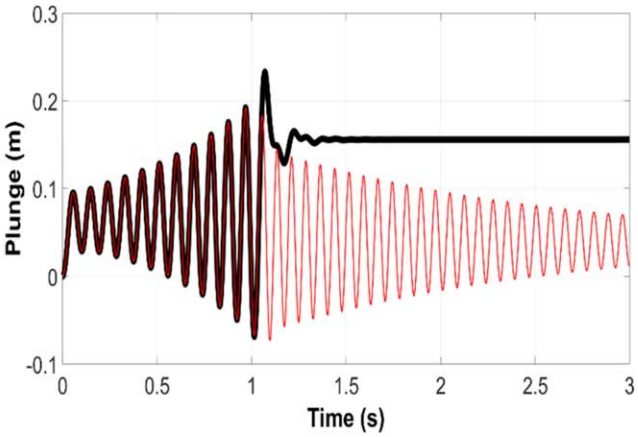

b. Wingtip plunge

Figure 19. Comparison between the Zigzag wingbox and the GNATSpar wing at 142.11 m s^{-1} and 1° AOA. At $t = 1$ s, the semi-span is retracted by 10% in 0.1 s (red thin curve for GNATSpar and black thick curve for Zigzag).

5.3. Zigzag versus GNATSpar

This subsection presents a comparison between the dynamic behaviour of the Zigzag Wingbox and the GNATSpar wing. Both wings are set at 1° angle of attack. In the first scenario both wings are operating at 137 m s^{-1} which is the flutter speed. After 1 s, the wing span is retracted by 10% in 0.1 s. It can be clearly seen from figure 18 that for the Zigzag Wingbox the wingtip oscillations damp out much faster than those associated with the GNATSpar wing. However as stated earlier, the bending rigidity drops significantly during retraction for the Zigzag Wingbox hence the much larger wingtip plunge displacement.

In the second scenario, both wings are set at 142.11 m s^{-1} (5 m s^{-1} above flutter speed). After 1 s. The wing span is retracted by 10% in 0.1 s. It can be seen from figure 19 that both wings are capable of loads alleviation but the Zigzag Wingbox offers the advantage of higher damping and therefore higher level of aeroelastic stability.

6. Conclusion

A time-domain, dynamic model has been developed to study the aeroelastic behaviour of compliant span morphing wings. The model focuses on uniform, cantilever, rectangular, compliant span morphing wings. The structure of the wing is represented using modal shape functions. Theodorsen's unsteady aerodynamic theory was used to estimate the aerodynamic loads. A Padé approximation of Theodorsen's transfer function was adopted to allow time-domain simulations. Different sensitivity studies were conducted to assess the impact of actuation rate, mass per unit span, bending and torsional rigidity on the flutter of span morphing wings. Furthermore, a number of scenarios were studied to assess the feasibility of span morphing as a flutter suppression device to expand the operating flight envelope. Finally, a comparison study between two promising span morphing concepts was performed, namely the Zigzag Wingbox and the GNATSpar wing. The study shows that the Zigzag Wingbox is a more effective flutter suppression device but results in large variation in the wingtip plunge displacement. Finally, it has been shown that span morphing can be used as an effective flutter

suppression device but the aeroelastic behaviour of the wing is very much dependent on the morphing mechanism/concept utilised and its details.

ORCID iDs

Rafic M Ajaj https://orcid.org/0000-0001-7125-1702

References

[1] Barbarino S, Bilgen O, Ajaj R M, Friswell M I and Inman D J 2011 A review of morphing aircraft *J. Intell. Mater. Syst. Struct.* **22** 823–77

[2] Ajaj R M, Beaverstock C S and Friswell M I 2016 Morphing aircraft: the need for a new design philosophy *Aerosp. Sci. Technol.* **49** 154–66

[3] Ajaj R M, Friswell M I, Saavedra Flores E I, Keane A J, Isikveren A T, Allegri G and Adhikari S 2014 An integrated conceptual design study using span morphing technology *J. Intell. Mater. Syst. Struct.* **25** 989–1008

[4] Ajaj R M, Friswell M I, Saavedra Flores E I, Little O and Isikveren A T 2012 Span morphing: a conceptual design study *20th AIAA/ASME/AHS Adaptive Structures Conf. (23–26 April) (Honolulu, Hawaii, USA AIAA-2012-1510*

[5] Weisshaar T A 2006 *Morphing Aircraft Technology—New Shapes for Aircraft Design* RTO-MP-AVT-141 Neuilly-sur-Seine, France

[6] Blondeau J and Pines D 2007 Design and testing of a pneumatic telescopic wing for unmanned aerial vehicles *J. Aircr.* **44** 1088–99

[7] Bae J S, Seigler T M and Inman D J 2005 Aerodynamic and aeroelastic characteristics of a variable-span morphing wing *J. Aircr.* **42** 528–34

[8] Ajaj R M, Saavedra Flores E I, Friswell M I, Allegri G, Woods B K S, Isikveren A T and Dettmer W G 2013 The Zigzag wingbox for a span morphing wing *Aerosp. Sci. Technol.* **28** 364–75

[9] Ajaj R M, Saavedra Flores E I, Friswell M I and DiazDelaO F A 2014b Span morphing using the compliant spar *J. Aerosp. Eng.* **28** 1–13

[10] Ajaj R M, Friswell M I, Bourchak M and Harasani W 2016 Span morphing using the GNATSpar wing *Aerosp. Sci. Technol.* **53** 38–46

[11] Woods B K S and Friswell M I 2015 The adaptive aspect ratio morphing wing: design concept and low fidelity skin optimization *Aerosp. Sci. Technol.* **42** 209–17

[12] Huang R and Qiu Z 2013 Transient aeroelastic responses and flutter analysis of a variable-span wing during the morphing process *Chin. J. Aeronaut.* **26** 1430–8

[13] Li W and Jin D 2018 Flutter suppression and stability analysis for a variable-span wing via morphing technology *J. Sound Vib.* **412** 410–23

[14] Oktay T and Sultan C 2014 Flight control energy saving via helicopter rotor active morphing *J. Aircr.* **51** 1784–804

[15] Theodorsen T 1935 General theory of aerodynamic instability and the mechanism of flutter *Technical Report No.* 496 NACA

[16] Brunton S L and Rowley C W 2011 Low-dimensional state-space representations for classical unsteady aerodynamic models *49th AIAA Aerospace Sciences Meeting Including the New Horizons Forum and Aerospace Exposition (Orlando, Florida)* AIAA-2011-476

[17] Breuker R D, Abdallah M, Milanese A and Marzocca P 2008 Optimal control of aeroelastic systems using synthetic jet actuators *49th AIAA/ASME/ASCE/AHS/ASC Structures, Structural Dynamics, and Materials Conf. (Illinois, USA)* AIAA-2008-1726

[18] Patil M J, Hodges D H and Cesnik C E S 2001 Nonlinear aeroelasticity and flight dynamics of high-altitude, long-endurance aircraft *J. Aircr.* **38** 88–94

[19] Patil M J, Hodges D H and Cesnik C E S 2000 Nonlinear aeroelastic analysis of complete aircraft in subsonic flow *J. Aircr.* **37** 753–60

[20] Raghavan B and Patil M J 2009 Flight dynamics of high aspect-ratio flying wings: effect of large trim deformation *J. Aircr.* **46** 1808–12

[21] Patil M J 1997 Aeroelastic tailoring of composite box beams *Proc. 35th Aerospace Sciences Meeting and Exhibit (Reno, Nevada)*

[22] Fung Y C 1993 *An Introduction to the Theory of Aeroelasticity* (New York: Dover) p 205